Inorg. Chem. **2007**, *46*, 3203–3211

Luminescence Functionalization of SBA-15 by $YVO_4:Eu^{3+}$ as a Novel Drug Delivery System

Piaoping Yang,[†] Shanshan Huang,[†] Deyan Kong,[†] Jun Lin,*[,†] and Honggang Fu[‡]

Key Laboratory of Rare Earth Chemistry and Physics, Changchun Institute of Applied Chemistry, Chinese Academy of Sciences, Changchun 130022, P. R. China, and School of Chemistry and Materials Science, Heilongjiang University, Harbin 150080, P. R. China

Received December 2, 2006

Luminescence functionalization of the ordered mesoporous SBA-15 silica was realized by depositing a $YVO_4:Eu^{3+}$ phosphor layer on its surface via the Pechini sol–gel process, resulting in the formation of the $YVO_4:Eu^{3+}$@SBA-15 composite material. This material, which combines the mesoporous structure of SBA-15 and the strong red luminescence property of $YVO_4:Eu^{3+}$, can be used as a novel functional drug delivery system. The structure, morphology, porosity, and optical properties of the materials were well characterized by X-ray diffraction, Fourier transform infrared spectroscopy, scanning electron microscopy, transmission electron microscopy, N_2 adsorption, and photoluminescence spectra. As expected, the pore volume, surface area, and pore size of SBA-15 decrease in sequence after deposition of the $YVO_4:Eu^{3+}$ layer and the adsorption of ibuprofen (IBU, drug). The IBU-loaded $YVO_4:Eu^{3+}$@SBA-15 system still shows the red emission of Eu^{3+} (617 nm, $^5D_0$–$^7F_2$) under UV irradiation and the controlled drug release property. Additionally, the emission intensity of Eu^{3+} increases with an increase in the cumulative released amount of IBU in the system, making the extent of drug release easily identifiable, trackable, and monitorable by the change of luminescence. The system has great potential in the drug delivery and disease therapy fields.

1. Introduction

In the past three decades, sustained/controlled drug delivery systems have attracted much attention in the fields of modern medice and pharmaceuticals because of their high drug delivery efficiency and reduced toxicity in comparison with conventionally administrated drugs in dosage forms.[1,2] In general, controlled drug delivery systems can not only deliver the therapeutic drugs to the targeted cells or tissues but also maintain the optimum concentration and rational toxicity of drugs in precise sites of the organs, which can improve therapeutic efficiency and reduce toxicity.[2] A large variety of polymer-based pharmaceutical carrier systems have been successfully employed as means of sustained/controlled drug delivery for their improved drug loading efficiency and degradable property.[3] Recently, ordered mesoporous silica materials have gained considerable attention as carriers for drugs because of their stable mesoporous structure, tunable pore size, high specific surface area with abundant Si−OH active bonds on the pore walls, nontoxic nature, well-defined

* To whom correspondence should be addressed. E-mail: jlin@ciac.jl.cn.
[†] Changchun Institute of Applied Chemistry.
[‡] Heilongjiang University.

(1) (a) Qu, F. Y.; Zhu, G. S.; Lin, H. M.; Sun, J. Y.; Zhang, D. L.; Li, S. G.; Qiu, S. L. *Eur. J. Inorg. Chem.* **2006**, 3943. (b) Song, S.-W.; Hidajat, K.; Kawi, S. *Langmuir* **2005**, *21*, 9568. (c) Yang, Q.; Wang, S. C.; Fan, P. W.; Wang, L. F.; Di, Y.; Lin, K. F.; Xiao, F. S. *Chem. Mater.* **2005**, *17*, 5999.

(2) (a) Guo, X.; Szoka, F. *Acc. Chem. Res.* **2003**, *36*, 335. (b) Kataoka, K.; Harada, A.; Nagasaki, Y. *Adv. Drug Delivery Rev.* **2001**, *47*, 113. (c) Rösler, A.; Vandermuelen, G. W. M.; Klok, H.-A. *Adv. Drug Delivery Rev.* **2001**, *53*, 95. (d) Uhrich, K. E.; Cannizzaro, S. M.; Langer, R. S.; Shakesheff, K. M. *Chem. Rev.* **1999**, *99*, 3181. (e) Kataoka, K. In *Controlled Drug Delivery: Challenges and Strategies*; Park, K., Ed.; American Chemical Society: Washington, DC, **1997**; pp 49−71. (f) Yokoyama, M.; Okano, T. *Adv. Drug Delivery Rev.* **1996**, *21*, 77.

(3) (a) Nasongkla, N.; Shuai, X.; Ai, H.; Weinberg, B. D.; Pink, J.; Boothman, D. A.; Gao, J. *Angew. Chem., Int. Ed.* **2004**, *43*, 6323. (b) Fu, J.; Fiegel, J.; Hanes, J. *Macromolecules* **2004**, *37*, 7174. (c) Lee, M.-R.; Baek, K.-H.; Jin, H. J.; Jung, Y.-G.; Shin, I. *Angew. Chem., Int. Ed.* **2004**, *43*, 1675. (d) Dalhaimer, P.; Engler, A. J.; Parthasarathy, R.; Discher, D. E. *Biomacromolecules* **2004**, *5*, 1714. (e) Haag, R. *Angew. Chem., Int. Ed.* **2004**, *43*, 278. (f) Bae, Y.; Fukushima, S.; Harada, A.; Kataoka, K. *Angew. Chem., Int. Ed.* **2003**, *42*, 4640. (g) Rösler, A.; Vandermuelen, G. W. M.; Klok, H.-A. *Adv. Drug Delivery Rev.* **2001**, *53*, 95. (h) Bae, Y. H.; Huh, K. M.; Kim, Y.; Park, K. H. *J. Controlled Release* **2000**, *64*, 3. (i) Ravi Kumar, M. N. V. *J. Pharm. Sci.* **2000**, *3*, 238. (j) Ulrich, K. E.; Cannizzaro, S. M.; Langer, R. S.; Shakesheff, K. M. *Chem. Rev.* **1999**, *99*, 3181.

10.1021/ic0622959 CCC: $37.00
Published on Web 03/20/2007

surface properties, and good biocompatibility.[4−8] So far, a large number of drug storage/release systems based on ordered mesoporous silicas have been reported.[1,6,7,9−12] Since the discovery of triblock copolymer-templated SBA-15 in 1998,[13] the adsorption and surface properties of this mesoporous material have been adjusted by anchoring a variety of functional groups onto the surface. This makes it have many potential applications, such as selective adsorption of noble metals[14] and immobilization of enzymes.[15,16] Most recently, SBA-15 has been investigated as a host material for drug storage and controlled release systems.[1,12,17]

Additionally, surface-functionalized mesoporous silica materials can be used as excellent hosts for a variety of guest molecules. Reports on mesoporous silica materials functionalized with superparamagnetism have demonstrated feasible applications in biomedical fields, including drug/gene delivery,[18] magnetic resonance imaging,[19] bioseparation,[20] tissue repairing,[21] thermal tumor therapy,[22] and stimuli-responsive controlled-release delivery.[23] It is worth noting that mesoporous materials functionalized with photoluminescence (PL) also have potential applications in the fields of drug delivery and disease diagnosis and therapy.[24,25] This is because these controlled drug delivery systems not only have high pore volumes for the storage and delivery of drugs but also possess photoluminescence properties which can be tracked to evaluate the efficiency of the drug release. Surface-functionalized mesoporous silica may be employed for qualitative and quantitative detection of disease position and drug release efficiency. Therefore, the design of mesoporous materials functionalized with photoluminescence properties and drug storage capabilities plays a key role in achieving this application. Although luminescence functionalization (using Y_2O_3:Eu^{3+}, rare earth complexes, etc.) of inorganic porous materials (including carbon nanotubes and mesoporous silicas) was reported in several publications,[24,25] these materials have never been really tested as drug storage/release

(4) (a) Zhao, D.; Feng, J.; Huo, Q.; Melosh, N.; Fredrickson, G. H.; Chmelka, B. F.; Stucky, G. D. *Science* **1998**, *279*, 548. (b) Kresge, C. T.; Leonowicz, M. E.; Roth, W. J.; Vartuli, J. C.; Beck, J. S. *Nature* **1992**, *359*, 710.

(5) (a) Han, Y.; Li, D.; Zhao, L.; Xiao, F.-S. *Angew. Chem., Int. Ed*. **2003**, *42*, 3633. (b) Han, Y.; Xiao, F.-S.; Wu, S. *J. Phys. Chem. B* **2001**, *105*, 7963. (c) Liu, Y.; Zhang, W.; Pinnavaia, T. J. *Angew. Chem., Int. Ed.* **2001**, *40*, 1255. (d) Liu, Y.; Zhang, W.; Pinnavaia, T. J. *J. Am. Chem. Soc.* **2000**, *122*, 8791.

(6) Tourné-Péteilh, C.; Lerner, D. A.; Charnay, C.; Nicole, L.; Begu, S.; Devoisselle, J. M. *ChemPhysChem* **2003**, *4*, 281.

(7) Muñoz, B.; Rámila, A.; Pérez-Pariente, J.; Díaz, I.; Vallet-Regí, M. *Chem. Mater*. **2003**, *15*, 500.

(8) (a) Barbé, C.; Bartlett, J.; Kong, L.; Finnie, K.; Lin, H. Q.; Larkin, M.; Calleja, S.; Bush, A.; Calleja, G. *Adv. Mater*. **2004**, *16*, 1949. (b) Cheng, Y. L.; Brian, T. G.; Dusan, M. J.; Dsenija, J.; Shu, X.; Srdija, J.; Victor, S. Y. L. *J. Am. Chem. Soc*. **2003**, *125*, 4451.

(9) (a) Qu, F. Y.; Zhu, G. S.; Huang, S. Y.; Li, S. G.; Sun, J. Y.; Zhang, D. L.; Qiu, S. L. *Microporous Mesoporous Mater*. **2006**, *92*, 1. (b) Qu, F. Y.; Zhu, G. S.; Lin, H. M.; Zhang, W. W.; Sun, J. Y.; Li, S. G.; Qiu, S. L. *J. Solid. Chem*. **2006**, *179*, 2027. (c) Qu, F. Y.; Zhu, G. S.; Huang, S. Y.; Li, S. G.; Qiu, S. L. *ChemPhysChem* **2006**, *7*, 400. (d) Zhu, Y. F.; Shi, J. L.; Chen, H. G.; Shen, W. H.; Dong, X. P. *Microporous Mesoporous Mater*. **2005**, *84*, 218. (e) Zhu, Y. F.; Shi, J. L.; Shen, W. H.; Dong, X. P.; Feng, J. W.; Ruan, M. L.; Li, Y. S. *Angew. Chem., Int. Ed*. **2005**, *44*, 5083.

(10) (a) Andersson, J.; Rosenholm, J.; Areva, S.; Lindén, M. *Chem. Mater*. **2004**, *16*, 4160. (b) Horcajada, P.; Rámila, A.; Pérez-Pariente, J.; Vallet-Regí, M. *Microporous Mesoporous Mater*. **2004**, *68*, 105. (c) Rámila, A.; Muñoz, B.; Pérez-Pariente, J.; Vallet-Regí, M. *J. Sol−Gel Sci. Technol*. **2003**, *26*, 1199. (d) Fu, Q.; Rama Rao, G. V.; Ista, L. K.; Wu, Y.; Andrzejewski, B. P.; Sklar, L. A.; Ward, T. L.; Lopez, G. P. *Adv. Mater*. **2003**, *15* (15), 1262. (e) Tourné-Péteih, C.; Brunel, D.; Bégu, S.; Chiche, B.; Fajula, F.; Lerner, D. A.; Devoissele, J. M. *New J. Chem*. **2003**, *27*, 1415. (f) Mal, N. K.; Fujiwara, M.; Tanaka, Y.; Taguchi, T.; Matsukata, M. *Chem. Mater*. **2003**, *15*, 3385.

(11) (a) Vallet-Regí, M.; Rámila, A.; Del Real, R. P.; Pérez-Pariente, J. *Chem. Mater*. **2001**, *13*, 308. (b) Cho, S.-B.; Nakanishi, K.; Kokubo, T.; Soga, N.; Ohtsuki, C.; Nakamura, T.; Kitsugi, T.; Yamamuro, T. *J. Am. Ceram. Soc*. **1995**, *78*, 1769. (c) Kokubo, T.; Kushitani, H.; Sakka, S; Kitsugi, T.; Yamamuro, T. *J. Biomed. Mater. Res*. **1990**, *24*, 721.

(12) (a) Yiu, H. H. P.; Wight, P. A. *J. Chem. Mater*. **2005**, *15*, 3690. (b) Doadrio, J. C.; Sousa, E. M. B.; Izquierdo-Barba, I.; Doadrio, A. L.; Pérez-Pariente, J.; Vallet-Regí, I. M. *J. Mater. Chem*. **2004**, *16*, 462. (c) Doadrio, A. L.; Sousa, E. M. B.; Doadrio, J. C.; Pérez-Pariente, J.; Izquierdo-Barba; Vallet-Regí, I. M. *J. Controlled Release* **2004**, *97*, 125. (d) Vallet-Regí, M.; Doadrio, J. C.; Doadrio, A. L.; Izquierdo-Barba, I.; Pérez-Pariente, J. *Solid State Ionics* **2004**, *172*, 435.

(13) Zhao, D. Y.; Huo, Q. S.; Feng, J. L.; Chmelka, B. F.; Stucky, G. D. *J. Am. Chem. Soc.* **1998**, *120*, 6024.

(14) (a) Kang, T.; Park, Y.; Yi, J. *Ind. Eng. Chem. Res*. **2004**, *43*, 1478. (b) Liu, A. M.; Hidajat, K.; Kawi, S.; Zhao, D. Y. *Chem. Commun*. **2000**, 1145.

(15) (a) Vinu, A.; Murugesan, V.; Hartmann, M. *J. Phys. Chem. B* **2004**, *108*, 7323. (b) Lei, J.; Fan, J.; Yu, C. Z.; Zhang, L. Y.; Jiang, S. Y.; Tu, B.; Zhao, D. Y. *Microporous Mesoporous Mater*. **2004**, *73*, 121. (c) Deere, J.; Magner, E.; Wall, J. G.; Hodnett, B. K. *Catal. Lett*. **2003**, *85*, 19.

(16) Corriu, R. J. P.; Mehdi, A.; Reye, C.; Thieuleux, C. *Chem. Commun*. **2002**, 1382.

(17) Highton, F. The Pharmaceutics of Ibuprofen. In *Ibuprofen. A Critical Bibliographic Review*; Rainsford, K. D., Ed.; Taylor and Francis: London, 1999; pp. 53.

(18) (a) Schillinger, U.; Brill, T.; Rudolph, C.; Huth, S.; Gersting, S.; Kroetz, F.; Hirschberger, J.; Bergemann, C.; Plank, C. *J. Magn. Magn. Mater*. **2005**, *293*, 501. (b) Neuberger, T.; Schoepf, B.; Hofmann, H.; Von Rechenberg, B. *J. Magn. Magn. Mater*. **2005**, *293*, 483. (c) Gupta, A. K.; Curtis, A. S. G. *J. Mater. Sci. Mater. Med*. **2004**, *15*, 493. (d) Scherer, F.; Anton, M.; Schillinger, U.; Henke, J.; Bergemann, C.; Kruger, A.; Gansbacher, B.; Plank, C. *Gene Ther*. **2002**, *9*, 102. (e) Lubbe, A. S.; Bergemann, C.; Brock, J.; McClure, D. G. *J. Magn. Magn. Mater*. **1999**, *194*, 149.

(19) (a) Perez, J. M.; O'Loughin, T.; Simeone, F. J.; Weissleder, R.; Josephson, L. *J. Am. Chem. Soc*. **2002**, *124*, 2856. (b) Perez, J. M.; Josephson, L.; O'Loughlin, T.; Hoegemann, D.; Weissleder, R. *Nat. Biotechnol*. **2002**, *20*, 816. (c) Bulte, J. W. M.; Douglas, T.; Witwer, B.; Zhang, S.-C.; Strable, E.; Lewis, B. K.; Zywicke, H.; Miller, B.; van Gelderen, P.; Moskowitz, B. M.; Duncan, L. D.; Frank, J. A. *Nat. Biotechnol.* **2001**, *19*, 1141. (d) Gellissen, J.; Axmann, C.; Prescher, A.; Bohndorf, K.; Lodemann, K. P. *Magn. Reson. Imaging* **1999**, *17*, 557.

(20) (a) Xu, C.; Xu, K.; Gu, H.; Zheng, R.; Liu, H.; Zhang, X.; Guo, Z.; Xu, B. *J. Am. Chem. Soc.* **2004**, *126*, 9938. (b) Wang, D.; He, J.; Rosenzweig, N.; Rosenzweig, Z. *Nano Lett.* **2004**, *4*, 409. (c) Gu, H.; Ho, P.-L.; Tsang, K. W. T.; Wang, L.; Xu, B. *J. Am. Chem. Soc*. **2003**, *125*, 15 702. (d) Doyle, P. S.; Bibette, J.; Bancaud, A.; Viovy, J.-L. *Science* **2002**, *295*, 2237.

(21) Gupta, A. K.; Gupta, M. *Biomaterials* **2005**, *26*, 3995.

(22) (a) Hirsch, L. R.; Stafford, R. J.; Bankson, J. A.; Sershen, S. R.; Rivera, B.; Price, R. E.; Hazle, J. D.; Halas, N. J.; West, J. L. *Proc. Natl. Acad. Sci. U.S.A.* **2003**, *100*, 13549. (b) Hilger, I.; Andra, W.; Hergt, R.; Hiergeist, R.; Schubert, H.; Kaiser, W. A. *Radiology* **2001**, *218*, 570. (c) Jordan, A.; Scholz, R;. Wust, P.; Schirra, H.; Schiestel, T.; Schmidt, H.; Felix, R. *J. Magn. Magn. Mater.* **1999**, *194*, 185.

(23) (a) Giri, S.; Trewyn, B. G.; Stellmaker, M. P.; Lin, Victor S.-Y. *Angew. Chem., Int. Ed*. **2005**, *44*, 5038. (b) Arruebo, M.; Galán, M.; Navascués, N.; Téllez, C.; Marquina, C.; Ibarra, M. R.; Santamaría, J. *Chem. Mater*. **2006**, *18*, 1911.

(24) Shi, D. L.; Lian, J.; Wang, W.; Liu, G. K.; He, P.; Dong, Z. Y.; Wang, L. M.; Ewing, R. C. *Adv. Mater*. **2006**, *18*, 189.

(25) (a) Lin, Y. S.; Wu, S. H.; Hung, Y.; Chou, Y. H.; Chang, C.; Lin, M. L.; Tsai, C. P.; Mou, C. Y. *Chem. Mater*. **2006**, *18*, 5170. (b) Sun, L. N.; Zhang, H. J.; Peng, C. Y.; Yu, J. B.; Meng, Q. G. *J. Phys. Chem. B* **2006**, *110*, 7249. (c) Xiong, L. M.; Shi, J. L.; Gu, J. L.; Li, L.; Huang, W. M.; Gao, J. H.; Ruan, M. L. *J. Phys. Chem. B* **2005**, *109*, 731. (d) Peng, C. Y.; Zhang, H. J. Yu, J. B.; Meng, Q. G.; Fu, L. S.; Li, H. R. *J. Phys. Chem. B* **2005**, *109*, 15278. (e) Sauer, J.; Marlow, F.; Spliethoff, B.; Schüth F. *Chem. Mater.* **2002**, *14*, 217. (f) Xu, W.; Liao, Y. T.; Akins, D. L. *J. Phys. Chem. B* **2002**, *106*, 11127. (g) Xu, W.; Akins, D. L. *J. Phys. Chem. B* **2002**, *106*, 1991.

systems to demonstrate their advantages in this area. Additionally, the organic−inorganic hybrid composites (luminescent lanthanide complex-grafted mesoporous SiO_2, such as MCM-41 and SBA-15)[25] might not be suitable for a drug-release system because of their toxicity (large organic molecule, containing a phenyl group) and inferior stability. Moreover, in comparison with most of reported non-silica luminescent material (such as Y_2O_3:Eu^{3+}-modified carbon nanotubes),[24] the mesoporous silica-based luminescent materials show stable porous structures, large pore volumes and diameters, large specific surface areas with a large number of Si−OH groups on the surface, which are suitable for loading a high quantity of drug molecules and which possess high sustained-release properties.

Herein, we propose a novel design to fabricate drug storage/release systems by incorporating YVO_4:Eu^{3+} nanophosphors onto the surface of mesoporous SBA-15 via Pechini sol−gel process.[26,27] The obtained composite materials were well characterized by XRD, FT-IR, N_2 adsorption/desorption analysis, SEM, TEM and HRTEM, and luminescence spectra. In addition, the luminescence-functionalized SBA-15 materials were used as drug-carriers to study the release properties in the release media of simulated body liquid based on its high pore volume, luminescence, and nontoxic properties. It is shown that the emission intensity of Eu^{3+} increases with the increasing cumulative released amount of the drug (IBU) in the system, making the extent of drug release be easily identified, tracked, and monitored by the change of luminescence.

2. Experimental Section

2.1. Materials and Synthesis. 2.1.1. Synthesis of SBA-15. The starting materials for the synthesis of SBA-15 included tetraethyl orthosilicate (TEOS, 99%, Beijing Chemical Regent Company, Beijing), hydrochloric acid (36−38%, Beijing Chemical Regent Company, Beijing), and $(EO)_{20}(PO)_{70}(EO)_{20}$ (P123, M_w = 5800, Aldrich), all of which were used without further purification. SBA-15 was synthesized according to the reported procedure using P123 as a structure-directing agent and TEOS as a silicon source.[13] Typically, 4.0 g of P123 was dissolved in 30.0 g of H_2O and 120.0 g of dilute HCl solution (2.0 M) with stirring at 35 °C. Then 8.5 g of TEOS was added dropwise to the solution with stirring, and the mixture was maintained at this temperature for 20 h. It was then crystallized at 80 °C for 20 h without stirring. The obtained material was filtered, washed, and dried in air at room temperature. The as-synthesized material was calcined from room temperature to 500 °C at a heating rate of 1 °C min^{-1} and kept at 500 °C for 6 h to remove the templates.

2.1.2. Functionalization of SBA-15 by YVO_4:Eu^{3+}. Deposition of the YVO_4:Eu^{3+} phosphor layer onto the surface of the template-free SBA-15 was prepared by a Pechini sol−gel process.[26,27] The doping concentration of Eu^{3+} was 5 mol % of Y^{3+} in YVO_4, which had been optimized in our previous work.[27] In a typical process, stoichiometric weights of Y_2O_3 (99.99%, Shanghai Yuelong Non-Ferrous Metals Limited), Eu_2O_3 (99.99%, Shanghai Yuelong Non-Ferrous Metals Limited), and NH_4VO_3 (99%, analytical reagent (AR), Tianjin Damao Chemical Instrument Company) were dissolved in dilute HNO_3 (AR grade) and then added to a water−ethanol solution (v/v = 1/7). Then citric acid (AR grade) with a molar ratio of 2:1 to metal ions was added as a chelating agent. Subsequently, polyethylene glycol (PEG, M_w = 10 000) was added as a cross-linking agent with a concentration of 0.04 g mL^{-1}. The mixture was stirred for 1 h to form a stable sol. Then desired amount of the template-free SBA-15 powder was added into the sol with stirring. The suspension was stirred for another 3 h, and then the resulting material was separated by centrifugation. After it was dried at 100 °C for 1 h, the sample was heated from room temperature to 500 °C with a heating rate of 1 °C min^{-1} and maintained at 500 °C for 2 h in air for the crystallization of YVO_4:Eu^{3+}. In this way, the luminescence-functionalized SBA-15 materials were obtained (denoted as YVO_4:Eu^{3+}@SBA-15).

2.1.3. Preparation of Drug Storage/Release System. The drug storage/release profile for YVO_4:Eu^{3+}@SBA-15 system was prepared according to the previous report.[11] Ibuprofen (IBU, purchased from Nanjing Chemical Regent Company) was selected as the model drug. Typically, 0.5 g of the YVO_4:Eu^{3+}@SBA-15 sample was added to 50 mL of a hexane solution of IBU with a concentration of 60 mg mL^{-1} at room temperature and soaked for 24 h with stirring in a vial which was sealed to prevent the evaporation of hexane. The IBU-loaded YVO_4:Eu^{3+}@SBA-15 sample, denoted as IBU−YVO_4:Eu^{3+}@SBA-15, was separated by centrifugation, and then dried at 60 °C for 12 h.

The *in vitro* delivery of IBU was performed by immersion of 0.3 g of the sample in the release media of simulated body fluid (SBF) with stirring, and the immersion temperature was kept at 37 °C. The ionic composition of the as-prepared SBF solution was similar to that of human body plasma with a molar composition of 142.0:5.0:2.5:1.5:147.8:4.2:1.0:0.5 for $Na^+/K^+/Ca^{2+}/Mg^{2+}/Cl^-/HCO_3^-/HPO_4^{2-}/SO_4^{2-}$ (pH 7.4).[11] The ratio of SBF to adsorbed IBU was kept at 1 mL mg^{-1}. The amount of IBU adsorbed onto the mesoporous SBA-15 was monitored by thermogravimetry (TG) and elemental analysis. As a comparison, the drug storage/release profile for the SBA-15 system was also studied in the manner described above.

The experimental process for the luminescence functionalization of SBA-15 by YVO_4:Eu^{3+}, the subsequent loading and release of the IBU drug, and the corresponding sample pellet photographs under the irradiation of 365 nm UV lamp in the dark are schematically shown in Scheme 1.

2.2. Characterization. X-ray power diffraction (XRD) was performed on a Rigaku-Dmax 2500 diffractometer using Cu Kα radiation (λ = 0.15405 nm). Fourier-transform IR spectra were recorded on a Perkin-Elmer 580B IR spectrophotometer using KBr pellet technique. N_2 adsorption/desorption isotherms were obtained on a Micromeritics 2020M apparatus. Pore size distribution was calculated from the adsorption branch of N_2 adsorption/desorption isotherm and the Barret−Joner−Halenda (BJH) method. The BET surface areas were determined using the data between 0.05 and 0.35 just before the capillary condensation, and the pore volume was obtained by the t-plot method. Thermogravimetry (TG) was carried out on a Netzsch Thermoanalyzer STA 409 with a heating rate of 5 °C min^{-1} in a N_2 atmosphere. The morphology and composition of the samples were inspected using a field emission scanning electron microscope (FESEM, XL30, Philips) equipped with an energy-dispersive X-ray spectrum (EDS, JEOL JXA-840). Transmission electron microscopy (TEM) and high-resolution transmission electron microscopy (HRTEM) micrographs were

(26) (a) Pechini, M. P. U. S. Patent 3330697, 1967. (b) Kakihana, M.; Yoshimura, M. *Bull. Chem. Soc. Jpn*. **1999**, *72*, 1427. (c) Kakihana, M.; Domen, K. *MRS Bull.* **2000**, *25* (9), 27.
(27) (a) Yu, M.; Lin, J.; Fang, J. *Chem. Mater*. **2005**, *17*, 1783. (b) Yu, M.; Lin, J.; Wang, Z.; Fu, J.; Wang, S.; Zhang, H. J.; Han, Y. C. *Chem. Mater*. **2002**, *14*, 2224.

Scheme 1. Schematic Diagram Showing the Experimental Process for the Luminescence Functionalization of SBA-15 by $YVO_4:Eu^{3+}$ and the Subsequent Loading and Release of the IBU Drug (Left Side), together with the Corresponding Sample Pellet Photographs for SBA-15 (Daylight) and $YVO_4:Eu^{3+}$@SBA-15, IBU−$YVO_4:Eu^{3+}$@SBA-15, and IBU-Released IBU−$YVO_4:Eu^{3+}$@SBA-15 under the Irradiation of a 365 nm UV Lamp in the Dark

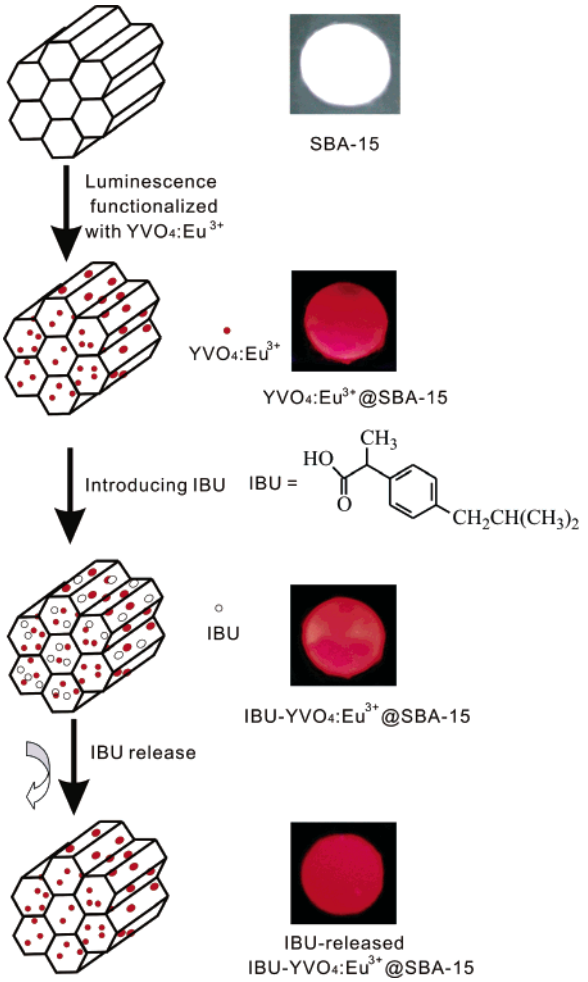

obtained from a FEI Tecnai G2 S-Twin transmission electron microscope with a field emission gun operating at 200 kV. Inductively coupled plasma (ICP) measurement (ICP-PLASMA 1000) was performed on the $YVO_4:Eu^{3+}$@SBA-15 sample to determine the exact loading level of $YVO_4:Eu^{3+}$ on the SBA-15 sample. The UV−vis excitation and emission spectra were obtained on a Hitachi F-4500 spectrofluorimeter equipped with a 150 W xenon lamp as the excitation source. All the measurements were performed at room temperature.

3. Results and Discussion

3.1. Formation, Structure, Morphology, and Properties of SBA-15, $YVO_4:Eu^{3+}$@SBA-15, and IBU−$YVO_4:Eu^{3+}$@SBA-15. 3.1.1. XRD. Figure 1 shows the low-angle XRD patterns of calcined SBA-15, $YVO_4:Eu^{3+}$@SBA-15, and IBU−$YVO_4:Eu^{3+}$@SBA-15. All the samples exhibit three well-resolved diffraction peaks that can be indexed as (100), (110), and (200) reflections associated with 2-D hexagonal symmetry (*P6mm*), confirming a well-ordered mesoporous structure in these material systems.[13] The results indicate that the ordered hexagonal mesoporous structure of SBA-15 remains intact after both the deposition of the YVO_4:

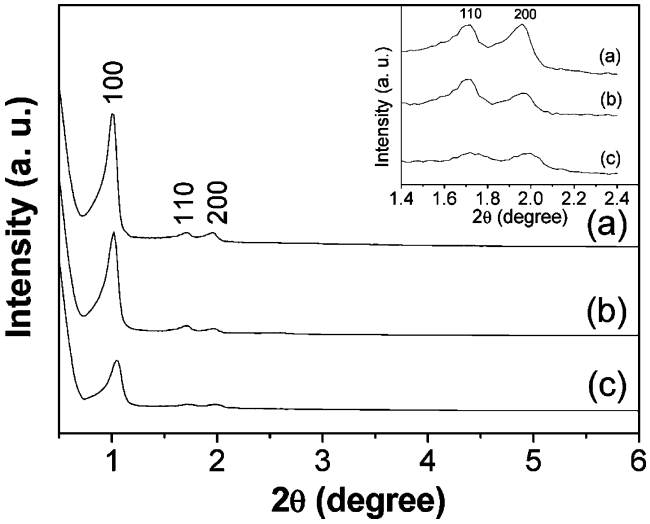

Figure 1. Low-angle XRD patterns of calcined SBA-15 (a), $YVO_4:Eu^{3+}$@SBA-15 (b), and IBU−$YVO_4:Eu^{3+}$@SBA-15 (c).

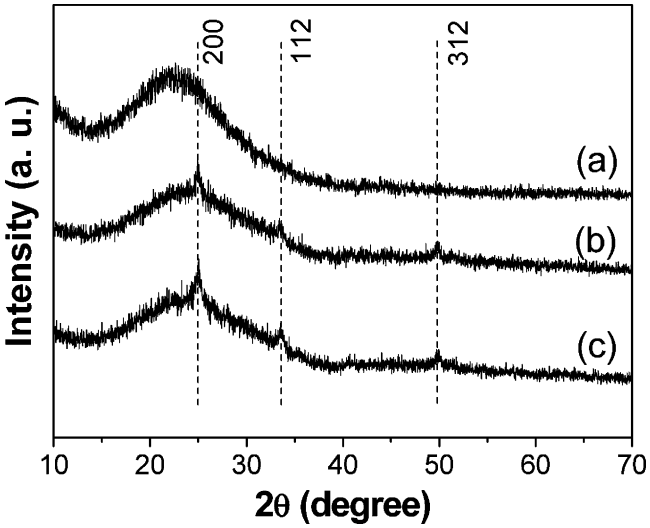

Figure 2. Wide-angle XRD patterns of calcined SBA-15 (a), $YVO_4:Eu^{3+}$@SBA-15 (b), and IBU−$YVO_4:Eu^{3+}$@SBA-15 (c).

Eu^{3+} phosphor layer and the adsorption of IBU. However, the intensity of these characteristic diffraction peaks decrease slightly after deposition of $YVO_4:Eu^{3+}$ and decrease further after the adsorption of IBU with respect to the bare SBA-15. This may be caused by the deposition of $YVO_4:Eu^{3+}$ and the incorporation of IBU molecules onto the mesoporous framework of SBA-15, which results in the decrease of crystallinity of the mesoporous materials.

Figure 2 displays the wide-angle XRD patterns of the corresponding samples. In Figure 2a for SBA-15, the broad band centered at $2\theta = 22°$ can be assigned to the characteristic reflection from amorphous SiO_2 (JCPDS 29-0085). While for $YVO_4:Eu^{3+}$@SBA-15 (Figure 2b) and IBU−$YVO_4:Eu^{3+}$@SBA-15 (Figure 2c), the typical characteristic diffraction peaks of YVO_4 (JCPDS 17−0341) can be observed at $2\theta = 25.0$, 33.5, and 49.5°, respectively, suggesting the successful crystallization of $YVO_4:Eu^{3+}$ on the surface of mesoporous SBA-15. The exact loading level of $YVO_4:Eu^{3+}$ on the SBA-15 sample was about 5.2 wt % (determined by ICP). The XRD results also demonstrate that the

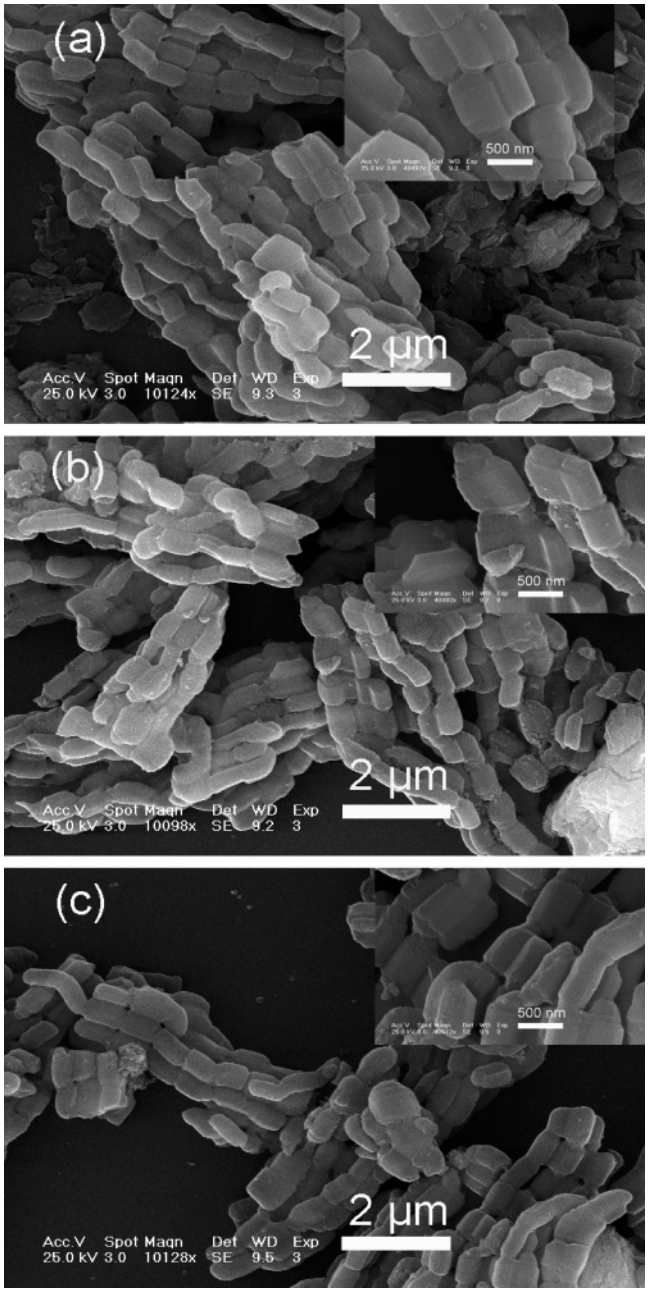

Figure 3. SEM images of the calcined SBA-15 (a), YVO_4:Eu^{3+}@SBA-15 (b), and IBU−YVO_4:Eu^{3+}@SBA-15 (c).

incorporation of IBU molecules into the pores of the mesoporous SBA-15 does not affect the crystalline structure of YVO_4, as shown in Figure 2c for IBU−YVO_4:Eu^{3+}@SBA-15.

3.1.2. SEM and TEM. Figure 3a−c shows the SEM images of calcined SBA-15, YVO_4:Eu^{3+}@SBA-15 and IBU−YVO_4:Eu^{3+}@SBA-15, respectively. It can be seen that all samples consist of relatively uniform rodlike particles about 0.5 μm in diameter and 1 μm in length, which aggregate into wheatlike microstructures as reported previously.[28] It seems that the introduction of YVO_4:Eu^{3+} and IBU has little influence on the surface morphology of SBA-15.

Figure 4 displays the representative TEM images of the calcined SBA-15 and YVO_4:Eu^{3+}@SBA-15 samples, respectively. The TEM images of SBA-15 (Figure 4a and b) exhibits the highly ordered hexagonal arrays of mesoporous channels, confirming a hexagonal (*P*6*mm*) mesostructure.[13] After deposition of YVO_4:Eu^{3+}, the TEM images for the YVO_4:Eu^{3+}@SBA-15 sample (Figure 4c and d) also exhibit a similar hexagonal array of ordered channels and the typical honeycomb, resembling that of SBA-15, indicating that mesostucture of SBA-15 is substantially conserved. The EDS result (Figure 4e) confirms the presence of silicon (Si), oxygen (O), yttrium (Y), and vanadium (V) in the YVO_4:Eu^{3+}@SBA-15 sample (the Au signal is from the Au coating for measurement). The Eu element was not detected clearly because of its low concentration (but it can be detected by the emission spectra, see post section). From the HRTEM image of YVO_4:Eu^{3+}@SBA-15 (Figure 4f), we can see crystalline phase (YVO_4) with well-resolved lattice fringes and some amorphous structure (SiO_2 in SBA-15). The distance (0.352 nm) between the adjacent lattice fringes just corresponds to the interplanar distance of the YVO_4 (200) planes, agreeing well with the *d*(200) spacing of the literature value (0.355 nm) (JCPDS No. 17-0341). These results further confirm the presence of crystalline YVO_4:Eu^{3+} on the surface of SBA-15, agreeing well with the XRD results.

3.1.3. FT-IR. The FT-IR spectra for IBU, SBA-15, YVO_4:Eu^{3+}@SBA-15, and IBU−YVO_4:Eu^{3+}@SBA-15 are depicted in Figure 5A and B, respectively. In the case of SBA-15 (Figure 5Aa), the obvious absorption bands from OH (3450 cm^{-1}), H_2O (1630 cm^{-1}), Si−O−Si (ν_s, 1100 cm^{-1}; ν_{as}, 807 cm^{-1}), Si−OH (ν_s, 950 cm^{-1}), and Si−O (δ, 471 cm^{-1}) (where ν_s represents symmetric stretching, ν_{as} asymmetric stretching, and δ bending) are present.[27,29] This indicates that a large number of the OH groups and H_2O present on the surface of SBA-15 play an important role in the bonding of metal ions from the impregnating sol and ibuprofen molecules from the ibuprofen−hexane solution. In Figure 5Ab for YVO_4:Eu^{3+}@SBA-15, the obvious absorption band at 833 cm^{-1} can be attributed to the vibration of V−O bond (in the VO_4^{3-} group), suggesting the formation of crystalline phase (YVO_4) on the surface of mesoporous silica during the heat treatment process.[26] In particular, this absorption band can still be clearly observed in the case of IBU−YVO_4:Eu^{3+}@SBA-15 (Figure 5Ac), which makes it possible to track it during the release process of transport in body fluids. Figure 5B shows the expanded FT-IR spectra between 1800 and 1300 cm^{-1}. It reveals that the intensity of ν(COOH) at 1718 cm^{-1} decreases significantly compared with that of ibuprofen (Figure 5Bd). Meanwhile, a new band centered at 1558 cm^{-1} is observed in Figure 5Bc, which can be attributed to the asymmetric stretching vibration of COO^-. These results indicate the interaction between the carboxylic group of ibuprofen and the Si−OH groups in the mesoporous silica. Furthermore, the absorption bands as-

(28) Margolese, D.; Melero, J. A.; Christiansen, S. C.; Chmelka, B. F; Stucky, G. D. *Chem. Mater*. **2000**, *12*, 2448.

(29) (a) Chen, Y.; Iroh, J. O. *Chem. Mater*. **1999**, *11*, 1218. (b) Kook Mah, S.; Chung, I. J. *J. Non-Cryst. Solids* **1995**, *183*, 252. (c) Kioul, A.; Mascia, L. *J. Non-Cryst. Solids* **1994**, *175*, 169.

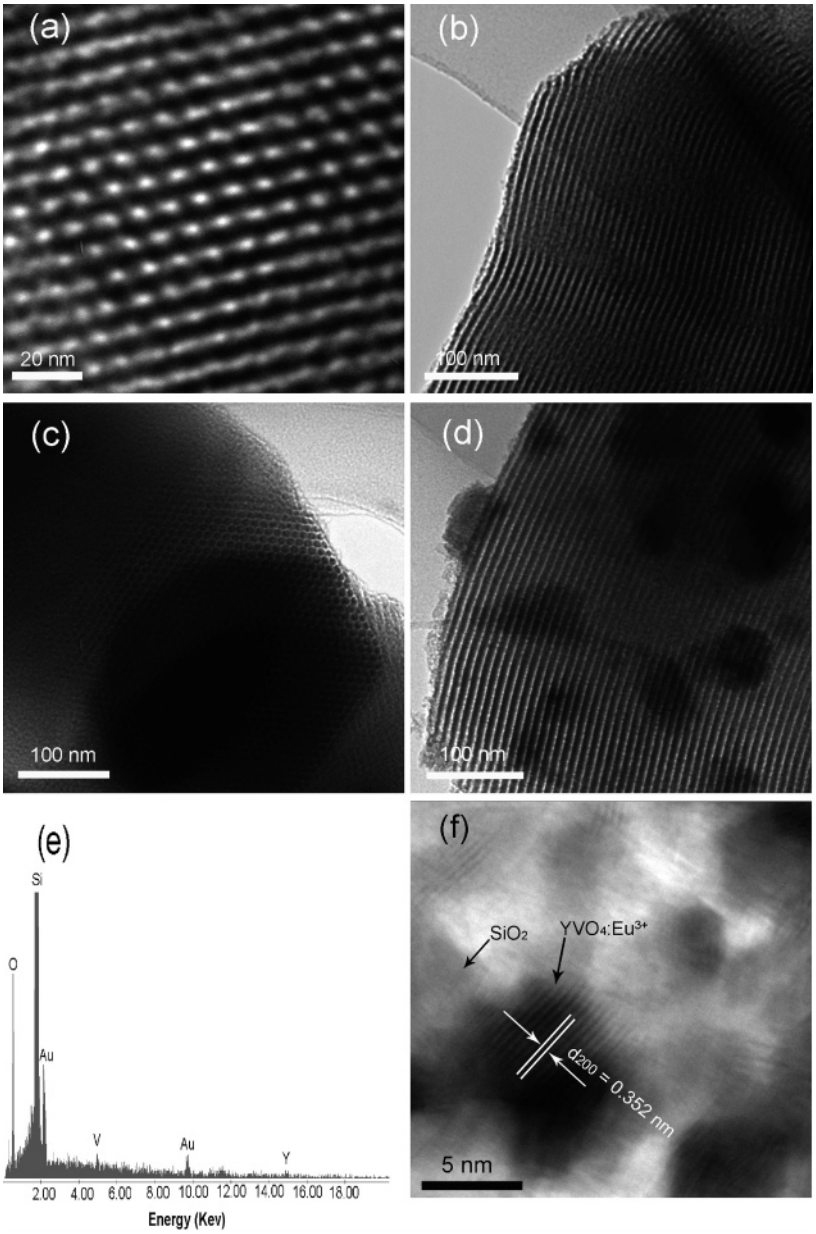

Figure 4. TEM images of calcined SBA-15 [(a) perpendicular to the pore axis, (b) parallel to the pore axis] and $YVO_4:Eu^{3+}$@SBA-15 [(c) perpendicular to the pore axis, (d) parallel to the pore axis], EDS of $YVO_4:Eu^{3+}$@SBA-15 (e), and the HRTEM image of $YVO_4:Eu^{3+}$@SBA-15 (f).

signed to the quaternary carbon atom located at 1463 and 1519 cm^{-1}, the tertiary carbon atom at 1379 cm^{-1}, the O−H bending vibration at 1421 cm^{-1}, and the C−H_x bond at 2920 and 2961 cm^{-1} [30] can be clearly observed in Figure 5Bc, which further confirms the successful incorporation of ibuprofen into the channels of the mesoporous silica. In addition, Figure 5A also reveals that the intensity of the OH groups at 3430 cm^{-1} and Si−OH at 950 cm^{-1} decreases after deposition of $YVO_4:Eu^{3+}$ and decreases further after ibuprofen loading. This observation further demonstrates the strong interaction between OH groups and the introduced components.

3.1.4. N_2 Adsorption/Desorption. Figure 6 shows the N_2 adsorption/desorption isotherms of calcined SBA-15 (a), $YVO_4:Eu^{3+}$@SBA-15 (b), IBU−$YVO_4:Eu^{3+}$@SBA-15 (c), and IBU-released IBU−$YVO_4:Eu^{3+}$@SBA-15 (d), and the corresponding pore size distributions are shown in Figure 7. As shown in the Figure 6, all the samples show typical IV isotherms with H_1-hysteresis, together with narrow size distributions (Figure 7), indicating a typical mesoporous material with hexagonal cylindrical channels.[13] Therefore, it can be deduced that the deposition of $YVO_4:Eu^{3+}$ and loading of IBU molecules have not greatly changed the pore structure of mesoporous SBA-15, which coincides with the XRD results. It can also be seen from Figure 6 that the marked uptake is located at a relative pressure close to 0.6. After deposition of $YVO_4:Eu^{3+}$ and incorporation of IBU, the marked uptakes move toward lower relative pressure as expected, located at about 0.5 and 0.4, respectively. The textural characteristics of the above four kinds of materials

(30) Bellamy, L. J. In *The Infrared Spectra of Complex Molecules*, 3rd ed.; Chapman and Hall: London, 1975; Vol. 2.

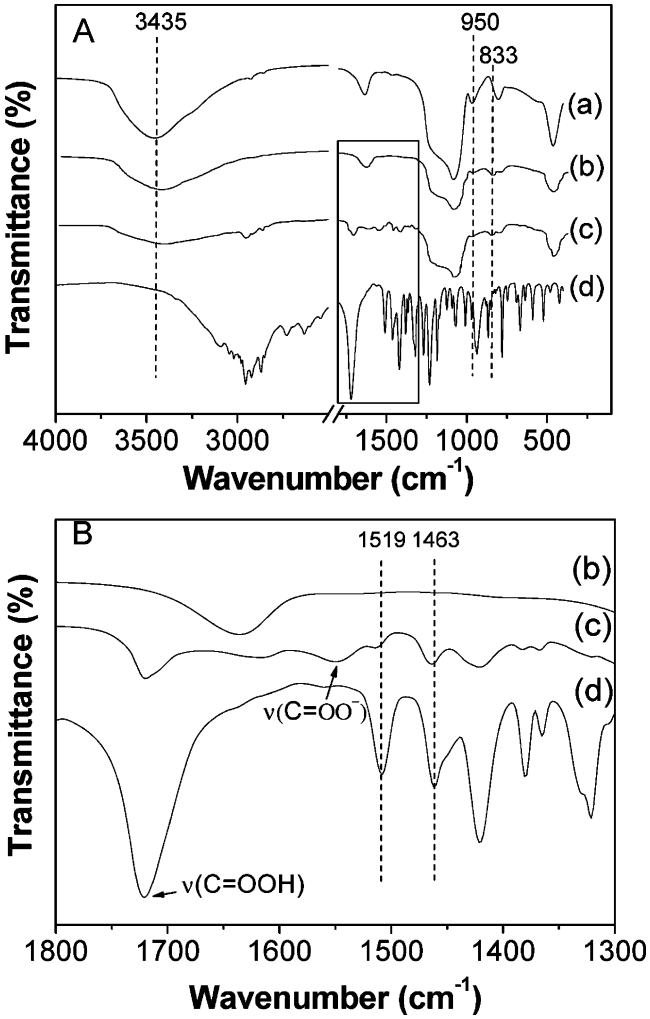

Figure 5. (A) FT-IR spectra of calcined SBA-15 (a), YVO_4:Eu^{3+}@SBA-15 (b), IBU−YVO_4:Eu^{3+}@SBA-15 (c), and IBU (d). (B) Expanded FT-IR spectra of YVO_4:Eu^{3+}@SBA-15 (b), IBU−YVO_4:Eu^{3+}@SBA-15 (c), and IBU (d).

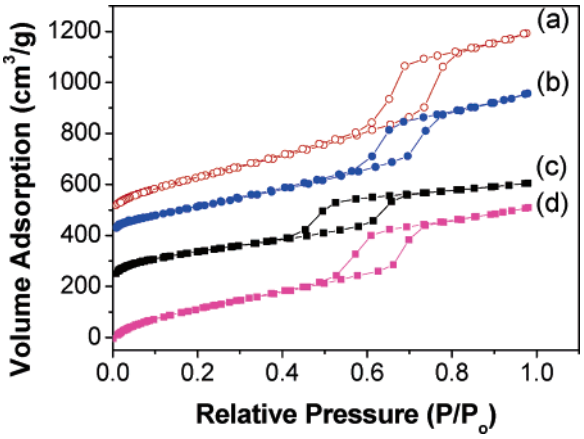

Figure 6. N_2 adsorption/desorption isotherms for calcined SBA-15 (a), YVO_4:Eu^{3+}@SBA-15 (b), IBU−YVO_4:Eu^{3+}@SBA-15 (c), and IBU-released IBU−YVO_4:Eu^{3+}@SBA-15 (d).

are summarized in Table 1. It is known from Table 1 that calcined SBA-15 has a high BET surface area (683 m^2 g^{-1}) and a large pore volume (1.15 cm^3 g^{-1}) and pore size (7.37 nm), indicative of its potential application as a host in a drug-release system. After the deposition of YVO_4:Eu^{3+}, the BET

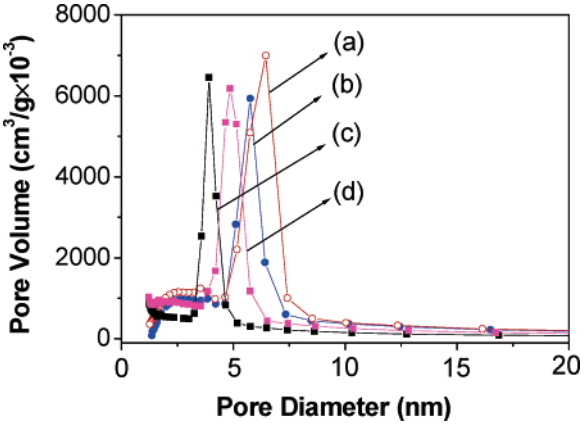

Figure 7. Pore size distribution for calcined SBA-15 (a), YVO_4:Eu^{3+}@SBA-15 (b), IBU−YVO_4:Eu^{3+}@SBA-15 (c), and IBU-released IBU−YVO_4:Eu^{3+}@SBA-15 (d).

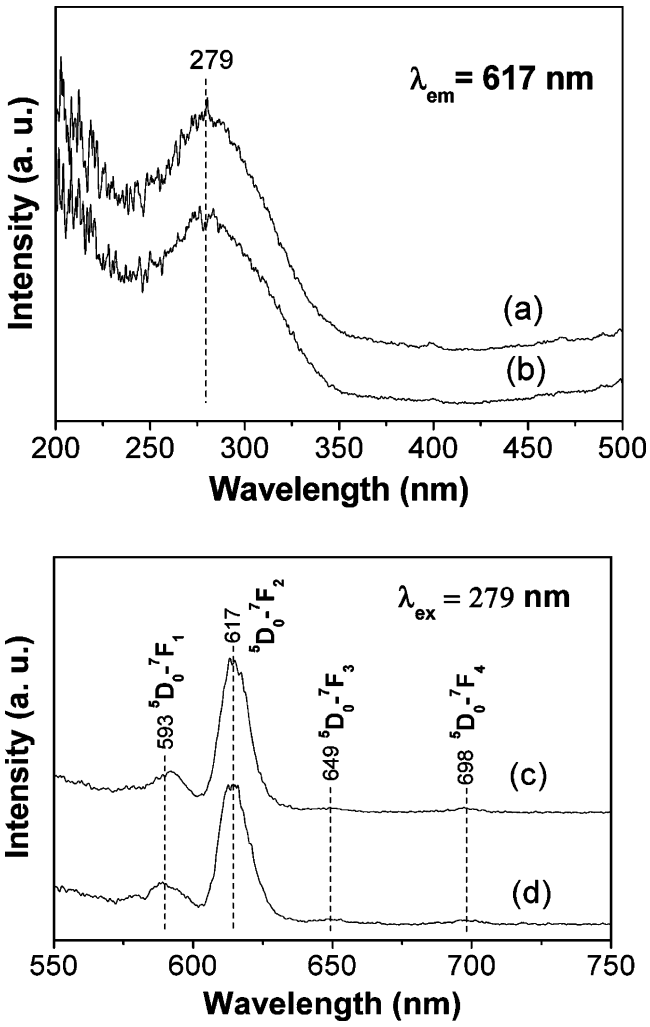

Figure 8. Excitation (a and b) and emission (c and d) spectra for YVO_4:Eu^{3+}@SBA-15 (a and c) and IBU− YVO_4:Eu^{3+}@SBA-15 (b and d).

surface area, pore volume, and pore size drop to 466 m^2 g^{-1}, 0.86 cm^3 g^{-1}, and 6.72 nm, respectively. As expected, the pore size and pore volume are reduced drastically after IBU adsorption compared with YVO_4:Eu^{3+}@SBA-15. These results further prove that IBU has been successfully incorporated into the channels of mesoporous SBA-15, which is consistent with above FT-IR results. Finally, it is worthwhile

Table 1. Textural Parameters of Calcined SBA-15, $YVO_4:Eu^{3+}$@SBA-15, and IBU−$YVO_4:Eu^{3+}$@SBA-15 and IBU-Released IBU−$YVO_4:Eu^{3+}$@SBA-15 Samples

samples	V_p ($cm^3\ g^{-1}$)	S_{BET} ($m^2\ g^{-1}$)	D (nm)
SBA-15	1.15	683	7.37
$YVO_4:Eu^{3+}$@SBA-15	0.86	466	6.72
IBU−$YVO_4:Eu^{3+}$@SBA-15	0.32	221	5.13
IBU-released IBU−$YVO_4:Eu^{3+}$@SBA-15	0.79	438	6.29

to point out that the sample still exhibits a typical IV isotherm after complete release of IBU, and the BET surface area, pore volume, and average pore diameter can almost be recovered (see Table 1 and Figure 7), indicating the good stability of this drug-release system.

3.1.5. Photoluminescence (PL) Properties. The photographs of SBA-15, $YVO_4:Eu^{3+}$@SBA-15, IBU−$YVO_4:Eu^{3+}$@SBA-15, and IBU-released IBU−$YVO_4:Eu^{3+}$ @SBA-15 under UV lamp irradiation (365 nm) are illustrated in Scheme 1. As shown in the scheme, strong red luminescence can be observed from $YVO_4:Eu^{3+}$@SBA-15 (whereas no emission can be observed from bare SBA-15), further indicating the successful introduction of $YVO_4:Eu^{3+}$ on SBA-15. After incorporation of IBU and complete release of IBU in SBF, the red luminescence can still be observed clearly (Scheme 1), demonstrating the good stability of this drug-storage/release system.

The PL properties of the samples were further characterized by excitation and emission spectra, respectively. The excitation spectra for $YVO_4:Eu^{3+}$@SBA-15 and IBU−$YVO_4:Eu^{3+}$@SBA-15 are shown in Figure 8a and b, respectively. The strong excitation band observed at 279 nm can be attributed to the VO_4^{3-} group.[27,31] No excitation peaks of Eu^{3+} resulting from its f → f transitions can be found because of their relatively low intensity with respect to that of VO_4^{3-} group. Therefore, it can be deduced that the excitation of Eu^{3+} is mainly caused by the energy transfer from VO_4^{3-} to Eu^{3+}, which is well consistent with our previous reports.[27] Upon excitation into the VO_4^{3-} at 279 nm, the characteristic transition lines from the excited $^5D_0$ level of Eu^{3+} can be observed in the emission spectra, as shown Figure 8c and d (the locations of the emission lines together with their assignments are labeled in the figure as well). In Figure 8c, the two main characteristic peaks observed in the red region originate from $^5D_0 \rightarrow {}^7F_1$ (593 nm) and $^5D_0 \rightarrow {}^7F_2$ (617 nm), respectively. It is worth noting that the characteristic emission peaks are still clearly observed in the emission spectrum of IBU−$YVO_4:Eu^{3+}$@SBA-15 (Figure 8d). This makes the drug loading system easily identifiable, trackable, and monitorable using the luminescence. A detailed relationship between the emission intensity and extent of IBU drug release in IBU−$YVO_4:Eu^{3+}$@SBA-15 system will be shown in next section.

3.2. Drug Storage/Release Properties. The respective IBU loading degrees of IBU for IBU-SBA-15 and IBU−$YVO_4:Eu^{3+}$@SBA-15 are 34 and 29 wt % determined by TG and elemental analysis (C loadings are 24.9 and 21.8%), respectively. The slightly higher degree of drug loading for

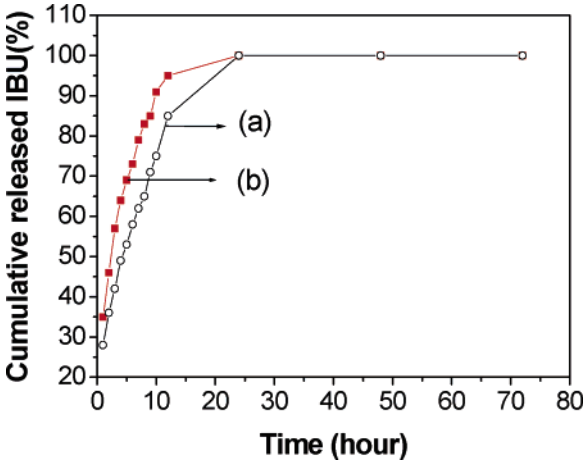

Figure 9. Cumulative IBU release from IBU-SBA-15 (a) and IBU−$YVO_4:Eu^{3+}$@SBA-15 (b) systems in the release media of SBF.

IBU-SBA-15 may be attributed to the higher surface area, larger pore size, and more silanol (Si−OH) groups on the surface of mesoporous silica, which is likely to form more hydrogen bonding with the carboxyl group of IBU. The cumulative drug release profiles of IBU−$YVO_4:Eu^{3+}$@SBA-15 and IBU-SBA-15 systems as a function of release time in the release media of SBF are shown in Figure 9, where all in vitro studies have been carried out under the same conditions. As shown in the figure, the release profiles are similar and clearly prove that both systems exhibit sustained-release properties. It can be observed in Figure 9a that the amount released from IBU-SBA-15 delivery system reaches about 36% in 2 h and 85% in 12 h. While for the IBU−$YVO_4:Eu^{3+}$@SBA-15 system (Figure 9b), about 46% of IBU has been released within 2 h, and the released amount reaches about 95% in 12 h. Both systems complete the release in 24 h. The slight difference in the release rate should mainly be attributed to the interaction between IBU molecules and Si−OH on the surface of mesoporous silica. As shown in the FT-IR spectra (Figure 5), the intensity of the Si−OH bands on the surface of SBA-15 decreases after the deposition of $YVO_4:Eu^{3+}$. Hence, the interaction between the carboxylic group of ibuprofen and the silanol groups on the surface of SBA-15 may be weakened, resulting in the acceleration of the release rate of ibuprofen molecules into the release media for the IBU−$YVO_4:Eu^{3+}$@SBA-15 system. In comparison with the IBU-SBA-15 system, the IBU−$YVO_4:Eu^{3+}$@SBA-15 drug-release system shows only slightly lower IBU storage capacity and IBU release rates in the release media, suggesting its potential applications in the area of drug delivery and disease therapy.

The PL emission intensity of IBU−$YVO_4:Eu^{3+}$@SBA-15 samples has been investigated as a function of cumulative released amount of IBU, as shown in Figure 10. It can be seen that the PL intensity increases with increasing the cumulative released amount of IBU, reaching a maximum when IBU is completely released from the drug storage system. It is well-known that the emission of Eu^{3+} will be quenched to some extent in the environments which contain

(31) Hsu, C.; Powell, R. C. *J. Lumin.* **1975**, *10*, 273.

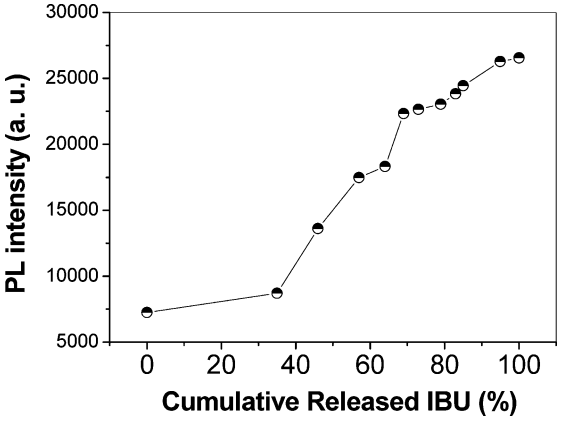

Figure 10. PL emission intensity of Eu^{3+} in IBU−YVO_4:Eu^{3+} @SBA-15 as a function of cumulative release amount of IBU.

high phonon frequency.[32] (For example, the emission of Eu^{3+} will be seriously quenched by OH groups with a vibrational frequency near 3450 cm^{-1}). The organic groups in IBU with tremendous vibration frequencies from 1000 to 3250 cm^{-1} will quench the emission of Eu^{3+} to a great extent in the IBU−YVO_4:Eu^{3+}@SBA-15 system. With the release of IBU, its quenching effect on the emission of Eu^{3+} will be weakened, resulting in an increase of emission intensity. This correlation between the emission intensity and drug release extent can be potentially used as a probe to monitor the drug-release process and efficiency in the course of the disease therapy.

(32) Blasse, G.; Grabmaier, B. C. *Luminescent Materials*; Springer-Verlag: Berlin, 1994; Chapter 4.

4. Conclusions

In summary, we have designed a novel drug-storage/release system functionalized with photoluminescence properties by deposition of a YVO_4:Eu^{3+} phosphor layer onto the channel surface of mesoporous SBA-15 (YVO_4:Eu^{3+}@SBA-15). This system possesses sustained-release properties of the drug in an in vitro assay. It exhibits strong red luminescence even after loading of the drug (IBU), and the PL intensity increases with increasing the cumulative released amount of IBU, reaching a maximum when IBU is completely released from the drug-storage system. The combination of both the drug storage/release and photoluminescence properties for YVO_4:Eu^{3+}@SBA-15 system makes it easy to identify, track, and monitor in the drug delivery and disease therapy process.

Acknowledgment. This project is financially supported by the foundation of "Bairen Jihua" of Chinese Academy of Sciences, the MOST of China (2003CB314707), and the National Natural Science Foundation of China (NSFC 50225205, 50572103, 20431030, 00610227).

IC0622959